Force Control of a Flexible Manipulator Based on the Measurement of Link Deflections

Jin-Soo Kim, Kuniaki Suzuki and Masaru Uchiyama
Department of Aeronautics and Space Engineering, Tohoku University

Abstract

In the past decade, a considerable amount of research has been devoted to flexible manipulators, especially to their modeling, vibration control, inverse kinematics and inverse dynamics. When a flexible manipulator is set to an environmental constraint, force control is necessary to be implemented to complete the task. In this work, we apply a concise position/force control scheme to a spatial flexible manipulator, using lumped-parameter modeling. The equations of motion, including elastic deflection and contact force, have been obtained based on the Hamilton's principle. Force control has been realized, both in simulation and experimentally. A comparison between those results is also presented.

1 Introduction

When a manipulator is set to an environmental constraint, not only a position control algorithm but also a force control algorithm is necessary to be implemented to complete the task. Because of that, in the past decade a considerable number of researches have been devoted to the force control algorithm of manipulators.

The approaches developed can be divided into active force control schemes and passive force control schemes, depending on whether a force sensor is being used or not. The former schemes control the contact force to the desired level using a force sensor [1], while the latter ones control the contact force as function of manipulator movements (position, velocity, acceleration) [2]. Active force control schemes, however, have some demerits. The schemes require expensive force sensors. Moreover, these force sensors are generally bulky and add an undesirable mass to the manipulator arm. As a result, controlling the vibration of flexible manipulator becomes a much more difficult job.

A force/torque sensor, generally mounted on the tip of the manipulator, consists of many strain gauges which measure the force/torque between a manipulator and the constraints. On the other hand, the use of strain gauges mounted on the links of manipulator to control the contact force/torque applied by the constraints is not very common.

Although flexible manipulators show some problems of stability [3] yet, they have the advantage of link flexibility. Some researchers have actively worked on force control of flexible manipulators [3]~[8], but almost all of them have passively applied the force control schemes of rigid manipulators to flexible ma-

nipulators, without using the relation between force and elastic deflection [3], [5].

Recently, very few publications appeared about force control algorithms which utilize elastic deflection and compliance of the links for control [6], [7]. Richter and Pfeiffer proposed a position/force control scheme for a flexible manipulator using strain gauges collocated on the links of the manipulator [6]. But, the application of this method is restricted to the trajectories on which the vibration of the end-effector of the manipulator is negligible. Kojima and Kawanabe have constructed a PIS control scheme for the constrained flexible manipulators. In that scheme, the deflections of the links are fed back to control the contact force [7].

In this paper, we aim at controlling the vibrations of the end-effector of a constrained, multi-link, flexible manipulator by controlling the constraint force. We apply the Hamilton's principle and the lumped-parameter modeling method to establish the dynamic equations and the relation between the elastic deflections of links and the contact force. Next a simple but effective scheme is proposed to control the constraint force and movements of the flexible manipulator. A precise simulation model is also developed using the commercial dynamic analysis software package ADAMS^{TM}. Finally, experiments and simulations are performed, and a comparison of the results is given to show the performance of our method.

2 Dynamic Modeling of Constrained Flexible Manipulators

2.1 Equations of motion

In this paper, we assume a flexible manipulator described by the generalized coordinates q,

$$q = \begin{bmatrix} \theta^T & e^T \end{bmatrix}^T,$$

where, $\theta \in \Re^n$ is the vector of the joint angles and $e \in \Re^m$ is the vector of the elastic deflections. We further assume that this flexible manipulator is set to an environmental constraint which is only rheonomous and can be expressed in the following form

$$\varphi(q, t) = 0, \tag{1}$$

where $\varphi : \Re^{n+m} \rightarrow \Re^1$ is a smooth constraint function, and t is time.

Using a lumped-parameter model of the flexible manipulator, the equation of motion can be derived based on the Hamilton's principle, and can be written as

$$\tau = M_{11}(q)\ddot{\theta} + M_{21}(q)\ddot{e} + h_1(q, \dot{q})$$
$$+ g_1(q) + J_{\varphi\theta}^T(q)\lambda \tag{2}$$

$$0 = M_{12}(q)\ddot{\theta} + M_{22}(q)\ddot{e} + h_2(q, \dot{q})$$
$$+ K_{22}e + g_2(q) + J_{\varphi e}^T(q)\lambda \tag{3}$$

where $M_{11} \in \Re^{n \times n}$, $M_{12} \in \Re^{n \times m}$, $M_{21} \in \Re^{m \times n}$ and $M_{22} \in \Re^{m \times m}$ are submatrices of the inertia matrix. h_1 and h_2 are vectors of centrifugal and Coriolis forces, g_1 and g_2 are gravity vectors, $K_{22} \in \Re^{m \times m}$ is stiffness matrix, $\lambda \in \Re^1$ is the Lagrange multiplier, $J_{\varphi\theta}$ and $J_{\varphi e}$ are Jacobian matrices for the constraints, and $\tau \in \Re^n$ is the joint torque vector.

In the equation of motion, two distinct parts can be recognized as Eq. (2) and Eq. (3). Equation (2) is related to the overall motion of the system, while Eq. (3) is related to the elastic motion.

Here, we use the Jacobian matrix for the above rheonomous constraints as

$$J_\varphi = \frac{\partial \varphi}{\partial p} J_q(q)$$
$$= \left[\begin{array}{ccccccccc} \frac{\partial \varphi}{\partial \theta_1} & \frac{\partial \varphi}{\partial \theta_2} & \cdots & \frac{\partial \varphi}{\partial \theta_n} & \frac{\partial \varphi}{\partial e_1} & \frac{\partial \varphi}{\partial e_2} & \cdots & \frac{\partial \varphi}{\partial e_m} \end{array} \right]$$
$$= \left[\begin{array}{cc} J_{\varphi\theta} & J_{\varphi e} \end{array} \right], \tag{4}$$

where $J_q = [J_\theta \; J_e]$ is the conventional Jacobian matrix of the manipulator, and p represents the Cartesian coordinates and the three Euler angles of the end-effector. The Lagrange multiplier can be represented as

$$\lambda = \frac{f_n}{|\text{grad}\varphi|},$$
$$\text{grad}\varphi = \nabla\varphi = \frac{\partial \varphi}{\partial p}, \tag{5}$$

where f_n is the component of the contact force normal to the constraints.

2.2 Computation of the constrain force

The elastic deflections of the flexible links are due to trajectory dynamics, contact force, gravity and friction. Neglecting the friction between the end-effector and the environmental constraint, the elastic deflections e can be obtained from Eq. (3) as

$$K_{22}e = -(D + g_2 + J_{\varphi e}^T\lambda) \tag{6}$$

where $D = M_{12}(q)\ddot{\theta} + M_{22}(q)\ddot{e} + h_2(q, \dot{q})$. For slow constrained motion, the sum of the gravitational and the constraint forces are much larger than the inertia forces. In that case, the term for the trajectory dynamics D can be neglected. Therefore, Eq. (6) is solved for λ as

$$\lambda = -(J_{\varphi e}^T)^+(K_{22}e + g_2) \tag{7}$$

where $(J_{\varphi e}^T)^+$ is the pseudo inverse of $J_{\varphi e}^T$. From the above equation it is evident that the contact force computation is configuration dependent. Moreover, when the manipulator moves slowly, the elastic deflections of the links are only dependent upon the contact forces and the gravitational force acting on them. The vibration of links can be easily controlled by controlling the contact forces.

3 Hybrid Position/Force Control Scheme

Most of industrial robotic manipulators have hardware velocity servo card in their controller in order to weaken the effect of nonlinearity of the system like friction, manipulator's inertia and so on. High ratio gear reduction also helps to weaken the effect of nonlinearity. In addition, high ratio reduction and high gain velocity servo produce very stable poles in the system. Due to such advantages, hardware velocity servo and high gear reduction are widely used. The relationship between velocity command and the produced torque can be written as

$$\tau = G_r K_{sp}(V_{ref} - K_{sv}\dot{\theta}_m),$$
$$= \Lambda(\dot{\theta}_c - \dot{\theta}), \tag{8}$$

where

G_r	:	gear reduction ratios,
K_{sp}	:	voltage feedback gains,
K_{sv}	:	voltage/velocity coefficients,
$\dot{\theta}_m = G_r\dot{\theta}$	:	angular velocities of motors,
V_{ref}	:	voltage velocity commands,
$\dot{\theta}_c$	:	velocity commands, and
$\Lambda = G_r{}^2 K_{sp} K_{sv}$	:	velocity feedback gains.

The voltage velocity commands V_{ref} are computed by

$$V_{ref} = G_r K_{sv}\dot{\theta}_c, \tag{9}$$

and are used in the experiments. The approximate joint velocities $\dot{\theta}_c$ can be computed as follows

$$\dot{\theta}_c = \dot{\theta}_t + \dot{\theta}_f, \tag{10}$$

where $\dot{\theta}_t$ is the joint velocity vector for positioning while $\dot{\theta}_f$ is an additional component for force control. The velocities $\dot{\theta}_t$ and $\dot{\theta}_f$ are respectively computed as

$$\dot{\theta}_t = J_\theta^{-1}(I - n^T n)K_{tp}(p_d - p),$$
$$\dot{\theta}_f = \Lambda^{-1}J_\theta^T n^T K_{fp}(\lambda_d - \lambda), \tag{11}$$

where I is the unit matrix. $n = \frac{\nabla\varphi}{|\nabla\varphi|}$ is the unit vector normal to the constraints. n^T, $(I - n^T n)$ define matrices which respectively select force and position directions. K_{tp} is a proportional gain matrix for positioning while K_{fp} is a proportional gain scalar for force control.

239

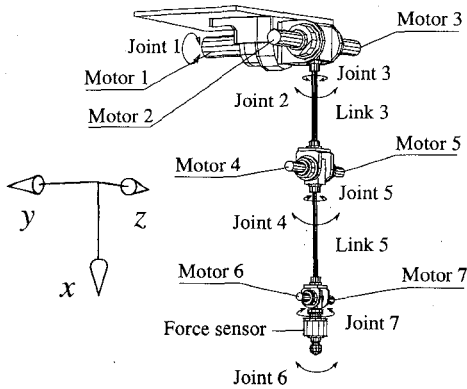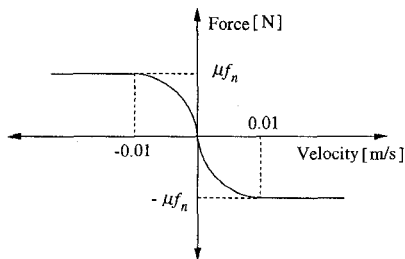Figure 1: Experimental robot with 2 links and 7 joints.

Figure 2: Friction force vs. velocity characteristic.

Figure 3: Lumped-parameter model of the experimental manipulator ADAM.

Table 1: ADAM link parameters.

	Link 3	Link 5
Length	0.5 m	0.5 m
Elastic part	0.359 m	0.394 m
Diameter	0.013 m	0.01 m
Material	SUP-6	SUP-6
EI	288.1 Nm^2	100.8 Nm^2
Mass	0.7 kg	0.5 kg

4 Application of the Proposed Scheme

To clarify the discussion, the motion of an experimental flexible manipulator ADAM (Aerospace Dual Arm Manipulator) is considered. ADAM has two arms, each arm of which consists of 2 elastic links and 7 rotary joints [10]. In this paper, however, only the left arm of ADAM (Fig. 1) is considered. The discussion is restricted to motion in joints 1, 2, 4 and 6 only while joint 6 always preserves an angle of $\pi/2$ [rad] with respect to the constraints.

Based on Eq. (7), experiments and simulations are performed. The results achieved by a precise model designed by the commercial dynamic analysis software package ADAMS$^{\text{TM}}$, are compared with the experimental results.

4.1 Simulation using ADAMS$^{\text{TM}}$

A precise model of the ADAM robot is constructed by ADAMS$^{\text{TM}}$. ADAMS$^{\text{TM}}$ is a commercial software package for dynamic analysis of mechanical systems produced by Mechanical Dynamics, Inc. In this simulator, a finite-element method based on Timosenko beam theory is used as a modeling method for flexible structures.

To obtain a precise model, the elastic beam is divided into five finite-elements. A simple model of Coulomb friction is included (Fig. 2) in order to obtain a realistic simulation model reflecting the exper-
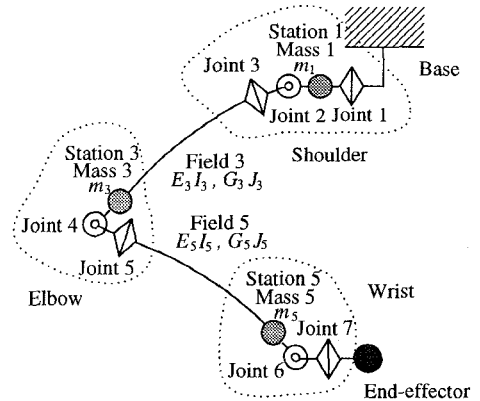
imental conditions. The model is recommended by uses of ADAMS$^{\text{TM}}$. As shown in Fig. 2, when the end-effector velocity becomes -0.01 and 0.01, friction forces become $-\mu f_n$ and μf_n, respectively, where μ is the friction constant.

4.2 Experiment

The experimental manipulator ADAM is driven by DC servo motors with velocity control. Each of the motors 1-3 has an optical encoder for sensing the joint angle and a tachometer for sensing the angular velocity. None of the motors 4-7 has a tachometer, and thus, pulse signals generated by optical encoders are transformed into velocity signals through F/V (Frequency to Voltage) converter.

The parameters of each link are presented in Table 1. The strain gauges are used to measure elastic deflections at the root of each link. In order to verify the accuracy of the contact force measured with the help of the strain gauges, a wrist force/torque is also attached to the tip of the manipulator

The arm under consideration is modeled by lumped-masses and massless springs as shown in Fig. 3 [9]. The lumped masses (stations) are considered concentrated at the tip of the respective links while the links themself are considered massless springs (fields) with elastic and torsional properties as $E_3 I_3$, $E_5 I_5$ and $G_3 J_3$, $G_5 J_5$, respectively. The joint angle vector
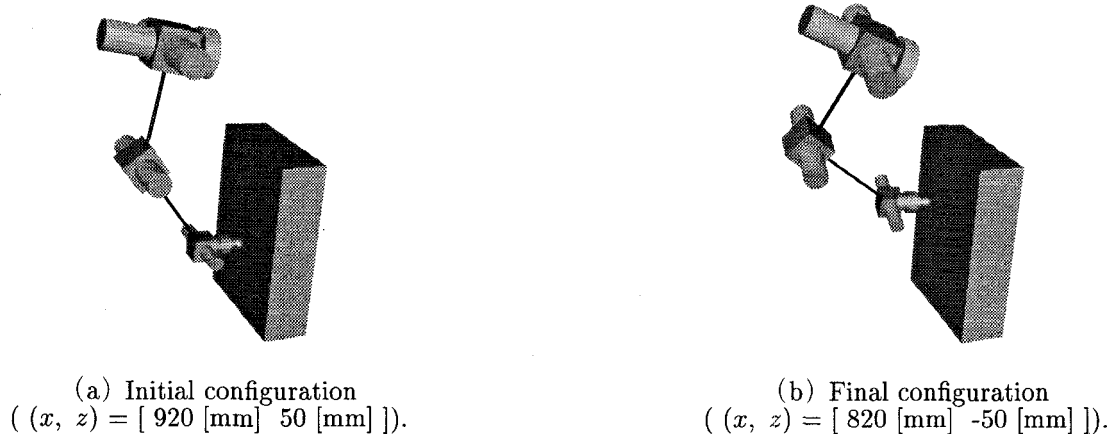
240

(a) Initial configuration
($(x, z) = [$ 920 [mm] 50 [mm]]).

(b) Final configuration
($(x, z) = [$ 820 [mm] -50 [mm]]).

Figure 4: ADAMS$^{\text{TM}}$ simulation.

θ and the link deflection vector e are:

$$\theta = [\theta_1 \quad \theta_2 \quad \theta_3 \quad \theta_4]^T \qquad (12)$$

$$e = [\delta_{y3} \quad \delta_{z3} \quad \delta_{y5} \quad \delta_{z5}]^T \qquad (13)$$

where δ_{y3}, δ_{y5}, δ_{z3} and δ_{z5} are elastic deflections along the y and z axis of link 3 and 5, respectively.

5 Results and Discussion

We present the experimental and simulation results for the case when the end-effector is not moving, and when it is moving while applying force. Figure 4 shows that the constraint is a vertical plane located at 0.375 [m] in the y direction from the robot's reference coordinate frame. So, the end-effector is constrained only in the y direction, whereas it is free to move in the $x - z$ plane. The responses of the manipulator while following the commanded paths on the above constraint, as obtained from simulations and experiments, are shown in Figs. 5 ~ 8. The parameters used in the experiments and simulations are presented in Table 2. The end-effector moves with velocities of 35.36 [mm/s], 70.71 [mm/s].

Table 2: Parameters for simulations and experiments

Terms	Parameter
K_{tp} [rad/(ms)]	diag[4.0, 4.0, 4.0]
K_{fp} [rad/(Ns)]	0.4
Desired force [N]	10 (y direction)
Sampling time [ms]	10

In order to justify the validity of f_e which is the force from Eq. (7), f is measured by the wrist force sensor at the same time. However, f used in the simulations is calculated by the IMPACT function of ADAMS$^{\text{TM}}$. For these simulations, K_{sp} of Eq. (8) is decided to be approximated to the one used in the experiments. The environmental stiffness and friction constants are taken as 10000 [N/m] and 0.2, respectively.

Figure 5 shows that when velocity of the end-effector is zero, f_e follows f exactly. However, when velocity is not zero, there is a small error between f and f_e which increases with the velocity. This is evident in the corresponding plots shown in Figs. 6 ~ 8. The reason of this error is the influence of the trajectory dynamics and the friction force which is neglected in Eq. (6) and Eq. (7).

In Figs. 6 and Fig 7, it is worthwhile to note that even when the tracking velocity is doubled, there is no considerable change in the vibrations. It is against the expected normal behavior and is because of the force feedback control which also suppresses the elastic vibrations.

To investigate the influence of friction, the simulations with $\mu = 0$ are performed. Figure 8 shows the responses of force and deflection for $\mu = 0$. If we compare Fig. 6 and Fig 7 with Fig. 8, it is clear that the friction affects the force responses considerably while the response errors are reduced when μ is taken as zero.

It is clear from Figs. 5 ~ 8 that the presented control scheme, which utilizes the relation between force and elastic deflection, is effective for constrained flexible manipulators modeled by the lumped-parameter modeling method.

6 Conclusions

For flexible manipulators, a hybrid position/force control scheme using the relation between force and elastic deflection has been presented. The control scheme has been studied for a 2-link 7-joint manipulator. Experimental results show that the system responses are in good agreement with simulation results. Investigating these results, it can be concluded that our control scheme is effective with some assumptions. The future work in this area may compensate the influence of the dynamic trajectory and friction force.

241

References

[1] M. H. Raibert and J. J. Craig, "Hybrid position/force control of manipulators," *Trans. ASME, J. of Dynamic System, Measurement and Control*, vol. 103, no. 2, pp. 126–133, 1981.

[2] M. T. Mason, "Compliance and force control for computer controlled manipulators," *IEEE Trans. on Systems, Man and Cybernetics*, vol. SMC-11, pp. 418–432 1981.

[3] B. C. Chiou and M. Shahinpoor, "Dynamics Stability Analysis of a One-Link Force-Controlled Flexible Manipulator," *J. Robotic Systems*, vol. 5, no. 5, pp. 443–451, 1988.

[4] T. Fukuda, "Flexibility control of elastic robotic arms," *J. Robotic Systems*, vol. 2, no. 1, pp. 73–88, 1985.

[5] F. Matsuno T. Asano and Y. Sakawa, "Modeling and Quasi-Static Hybrid Position/Force Control of a Constrained Planar Two-Link Flexible Manipulator," *IEEE Trans. on Robotics and Automation*, vol. 10, no. 3, pp. 287–297, 1994.

[6] F. Richter andF. Pfeiffer, "A Flexible Link Manipulator as a Force Measuring and Controlling Unit," *Proc. of the IEEE Int. Conf. on Robotics and Automation*, vol. 2, pp. 1214–1219, 1991.

[7] H. Kojima and T. Kawanabe, "Position and Force Control of Flexible Robot Arm with PIS Control," *J. Robotics Society of Japan*, vol. 10, no. 3, pp. 353–360, 1992 (in Japanese).

[8] J. S. Kim, K. Suzuki, A. Konno and M. Uchiyama "Force Control of Constrained Flexible Manipulators," *Proc. of the IEEE Int. Conf. on Robotics and Automation*, Vol. 1, pp. 635–640, 1996.

[9] A. Konno and M. Uchiyama, "Modeling of a Flexible Manipulator Dynamics Based on the Holzer's Method," *J. Robotics Society of Japan*, vol. 12, no. 7, pp. 1021–1028, 1994 (in Japanese).

[10] M. Uchiyama, A. Konno, T. Uchiyama, and S. Kanda, "Development of a flexible dual-arm manipulator testbed for space robotics," *Proc. of the IEEE Int. Workshop on Intelligent Robotics and Systems'90*, pp. 375–381, Tsuchiura, Japan, 1990.
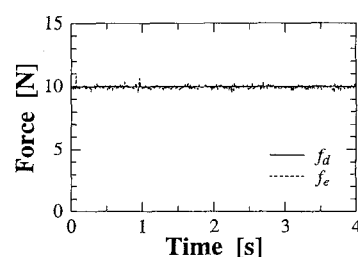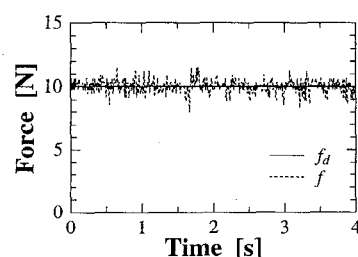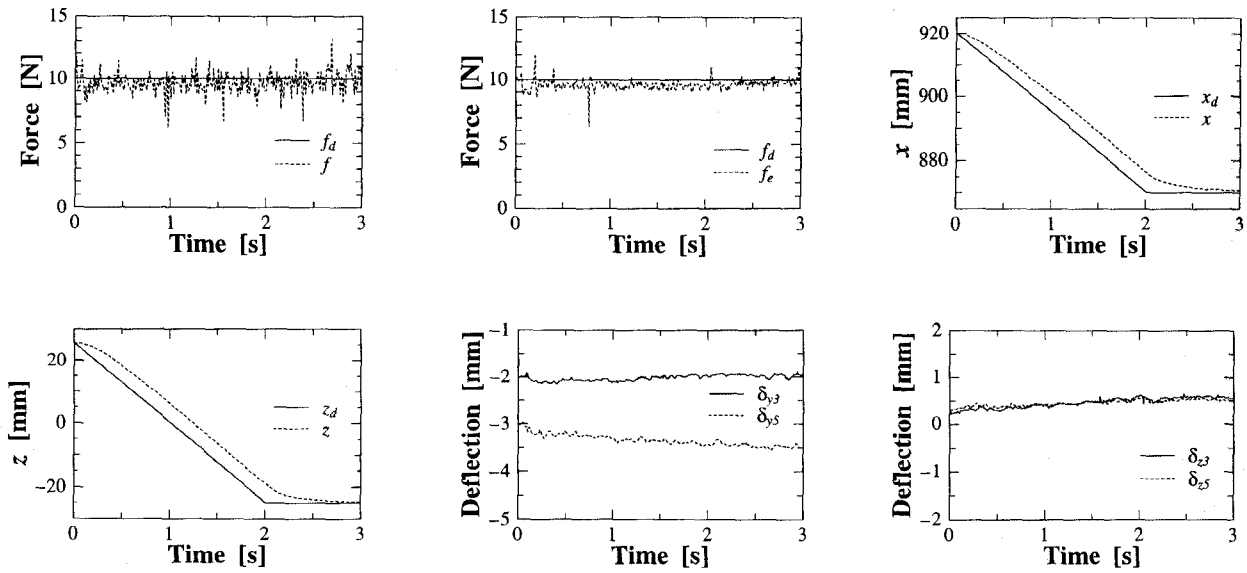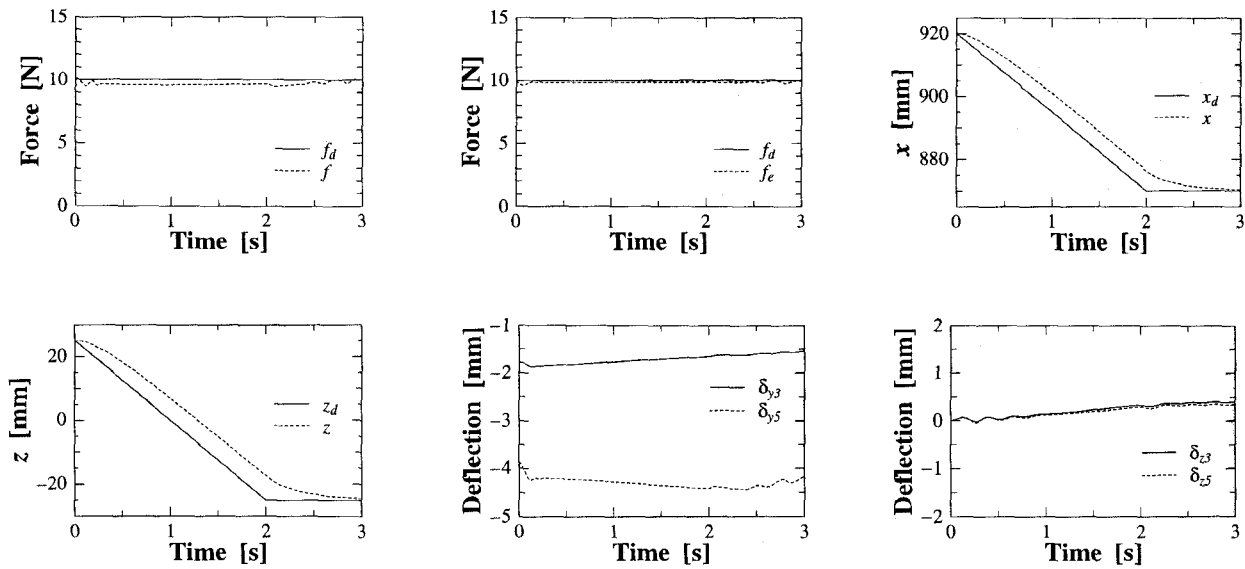
(a) Experimental result
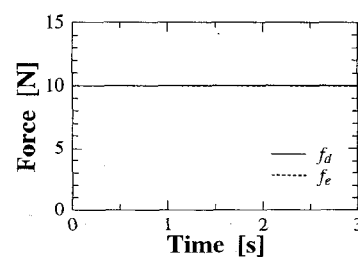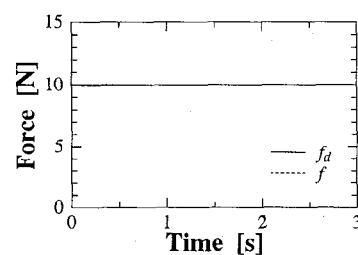
(b) Simulation result

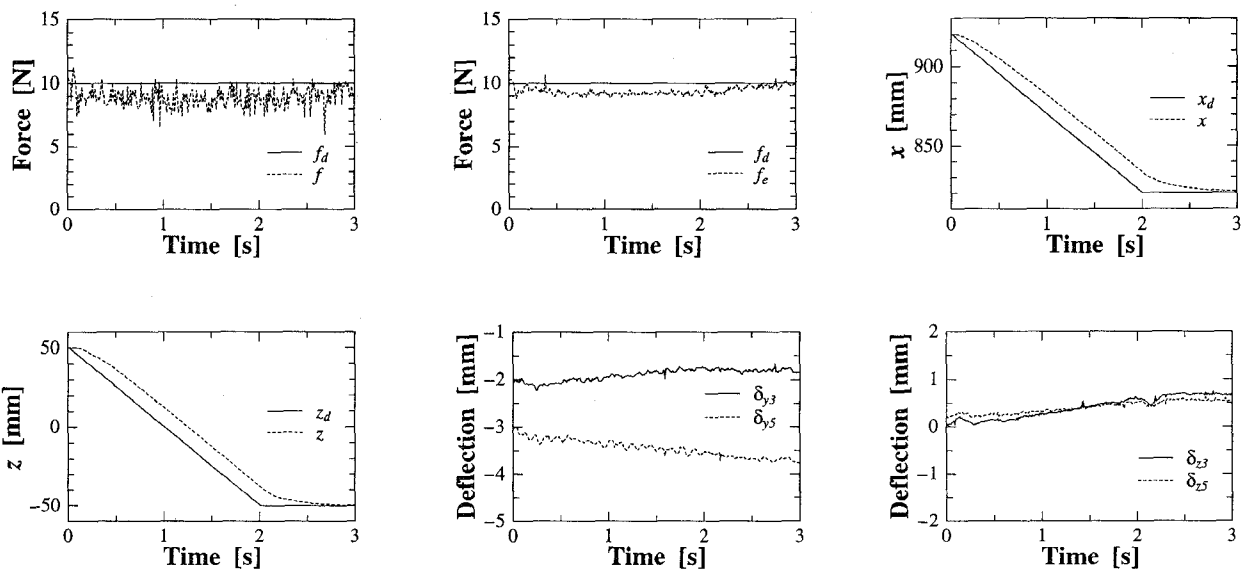Figure 5: When the end-effector of the robot does not move.

242

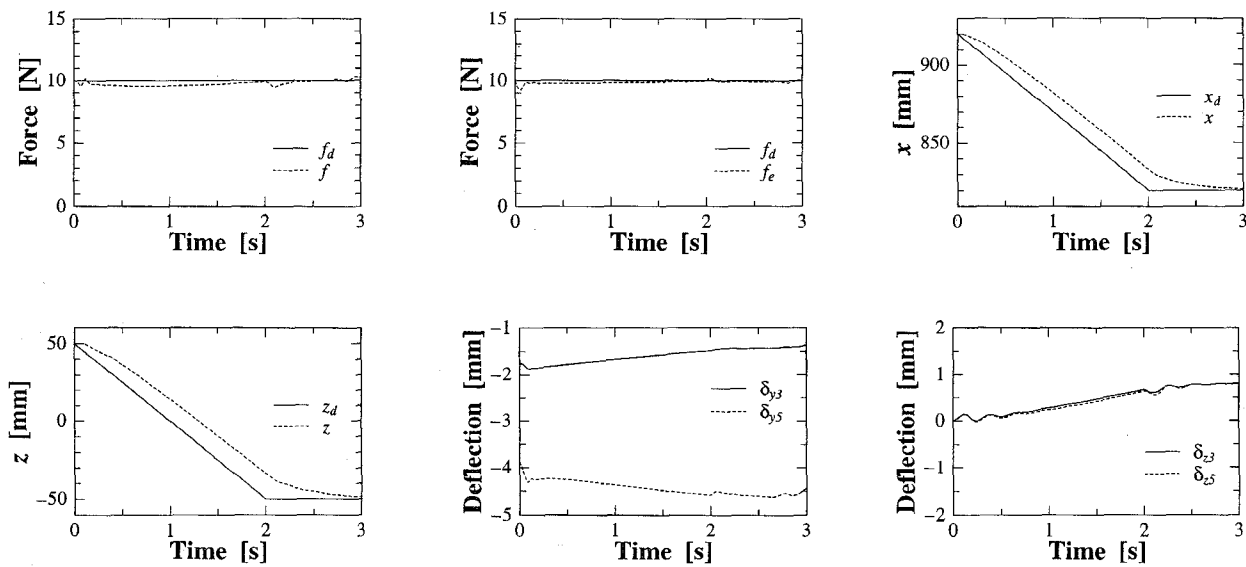(a) Experimental result

(b) Simulation result

Figure 6: When the end-effector of the robot moves by 35.36 [mm/s].
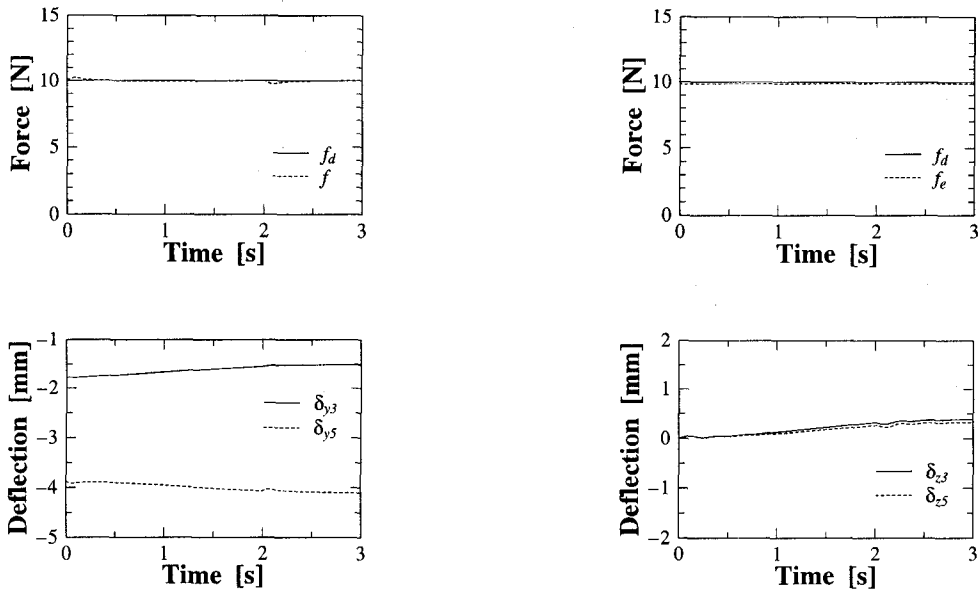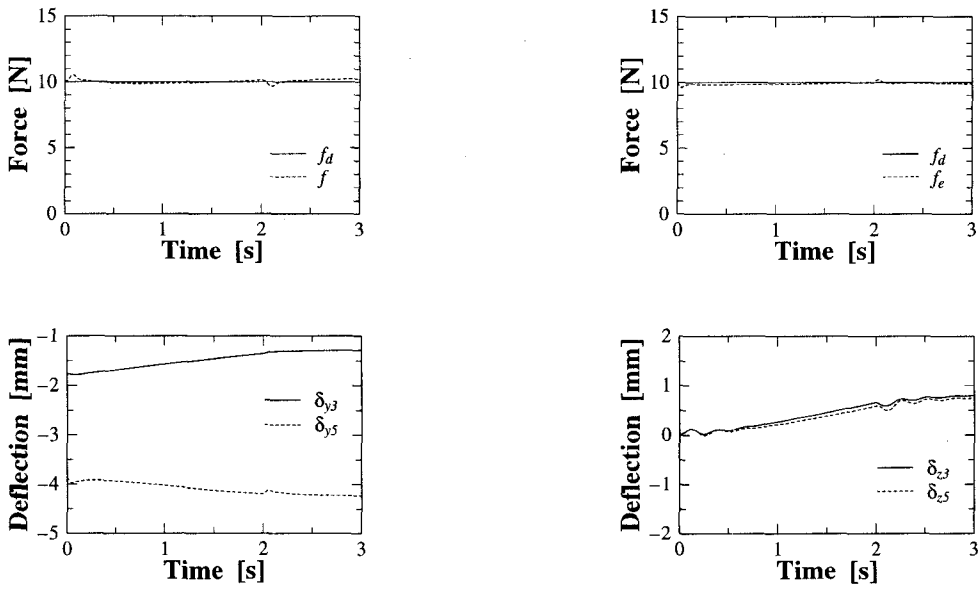
243

(a) Experimental result

(b) Simulation result

Figure 7: When the end-effector of the robot moves by 70.71 [mm/s].

244

(a) When the end-effector of the robot moves by 35.36 [mm/s].

(b) When the end-effector of the robot moves by 70.71 [mm/s].

Figure 8: Simulation for the case $\mu = 0$.

245